

1 **Variations of solar electron and proton flux in magnetic cloud**
2 **boundary layers and comparisons with those across the shocks**
3 **and in the reconnection exhausts**

4 Y. Wang^{1,2}, F. S. Wei¹, X. S. Feng¹, P. B. Zuo¹, J. P. Guo¹, X. J. Xu³ and Z. Li^{4,5}

5
6 *1 SIGMA Weather Group, State Key Laboratory for Space Weather, National Space Science Center, Chinese*
7 *Academy of Sciences, Beijing, 100190, China; yw@spaceweather.ac.cn*

8 *2 College of Earth Science, Graduate University of the Chinese Academy of Sciences, Beijing 100049, China*

9 *3 Institute of Space Science and Technology, Nanchang University, Nanchang 330031, China*

10 *4 National Key Laboratory of Science and Technology on Aerospace Flight Dynamics, Beijing, China, 100049*

11 *5 Beijing Aerospace Control Center, Beijing 100094, China*

12

13 **Abstract** Magnetic cloud boundary layer (BL) is a dynamic region formed by the interaction of the
14 magnetic cloud (MC) and the ambient solar wind. In the present study, we comparatively investigate
15 the proton and electron mean flux variations in the BL, in the interplanetary reconnection exhaust
16 (RE) and across the MC-driven shock by using the Wind 3DP and IMF data from 1995 to 2006. In
17 general, the proton flux has higher increments at lower energy bands compared with the ambient
18 solar wind. Inside the BL, the core electron flux increases quasi-isotropically and the increments
19 decrease monotonously with energy from $\sim 30\%$ (at 18 eV) to $\sim 10\%$ (at 70 eV); the suprathermal
20 electron flux usually increases in either parallel or antiparallel direction; the correlation coefficient of
21 electron flux variations in parallel and antiparallel directions changes sharply from ~ 0.8 below 70 eV
22 to ~ 0 above 70 eV. Similar results are also found for RE. However, different phenomena are found
23 across the shock where the electron flux variations first increase and then decrease with a peak
24 increment ($>200\%$) near 100 eV. The correlation coefficient of electron flux variations in parallel and
25 antiparallel directions is always around 0.8. The similar behavior of flux variations in BL and RE
26 suggest that reconnection may commonly occur in BL. Our work also implies that the strong energy
27 dependence and direction selectivity of electron flux variations, which are previously thought to have
28 no enough relevance to magnetic reconnection, could be considered as an important signature of
29 solar wind reconnection in the statistical point of view.

30

31 **Key words:** solar wind, plasmas, magnetic reconnection, coronal mass ejections, shock waves,
32 turbulence, acceleration of particles

33 **1 Introduction**

34 Magnetic clouds (MCs) are large-scale transient structures in the solar wind. In the past few
35 decades, problems about their solar origin, magnetic field and plasma structures have been widely
36 investigated (Bothmer & Schwenn 1994; Burlaga et al. 1980; Burlaga et al. 1981; Farrugia et al.
37 1994; Lepping et al. 2006; Lepping et al. 1997). In addition, as a subset of the Interplanetary Coronal
38 Mass Ejections (ICMEs), the propagation of MCs in interplanetary space is also an important issue in
39 heliospheric physics research. For example, a MC could be overtaken by a corotating stream that
40 would compress the plasma and field and make its tail region turbulent (Lepping, et al. 1997). There
41 might also be magnetic holes, directional discontinuities or reconnection layers in the front boundary
42 of the MCs (Janoo et al. 1998). Therefore, the interaction between the MC body and the ambient
43 solar wind seems to be a complex problem which not only aggravates the difficulty to understand the
44 evolution of ICME but also increases the complexity to identify the MC boundary (Wei et al. 2006;
45 Wei et al. 2003b).

46
47 Up to now, there is still no consistency among the criteria to identify the MC boundary such as
48 the temperature decrease, density decrease, directional discontinuity, magnetic hole and bidirectional
49 streaming of suprathermal electrons, as pointed out by many researchers (Burlaga et al. 1990;
50 Fainberg et al. 1996; Farrugia et al. 2001; Osherovich et al. 1993; Wei, et al. 2006; Wei et al. 2003a;
51 Wei, et al. 2003b; Wei et al. 2003c). Wei et al. (2003b) statistically analyzed the boundary physical
52 states of 80 MCs detected from 1969 to 2001 and suggested that the MC boundary is a complex
53 boundary layer (BL) formed by the interactions between the MC and the background solar wind,
54 rather than a simple discontinuity. The BL ahead of MC is called the front BL, while the following

55 one is the tail BL (Wei, et al. 2003b). For each BL, its outer boundary (M) is usually identified by the
56 magnetic field intensity drop, the abrupt change of field angle, and is accompanied with the
57 “three-high state” in the plasma beta value, temperature and density, while the inner boundary (G),
58 which separates the interaction region from the MC body, is usually associated with the “three-low
59 state” also in the plasma beta value, temperature and density (Wei, et al. 2003b). The MC detected by
60 Wind on 15 May 1997 provides a typical sample to reveal the BL’s properties (see Figure 1). The
61 spacecraft at 1 AU observed in sequence the MC-driven shock (if there is), the front BL and MC
62 body. As seen in the Figure, the magnetic field, plasma temperature and density behaviors inside the
63 BL, which is separated by the obvious boundaries (labeled by M_f and G_f , the subscript ‘f’ means
64 front), are completely different from those in the nearby upstream solar wind, the following MC
65 body and the preceding shock (sheath) region. Previous analyses show that the BL is often a unique
66 structure exhibiting decreased magnetic field as well as heated and accelerated plasma. These
67 features are preliminarily interpreted to be associated with the magnetic reconnection process since
68 they are important manifestations that could be often observed in a magnetic reconnection region
69 (Wei, et al. 2006; Wei, et al. 2003c).

70

71 Magnetic reconnection is an important process that can convert magnetic energy into thermal
72 and kinetic energy. Many researchers have intensively studied its dynamics in geo-magnetosphere
73 and solar corona, but the magnetic reconnection phenomena in the solar wind has drawn relatively
74 less attention so far. Early study suggested that interactions between a fast ICME and the ambient
75 solar wind might cause reconnection at the compressed leading boundary region of the ICME
76 (McComas et al. 1994). Recently, observations of reconnections at both leading and trailing

77 boundaries of interplanetary small-scale magnetic flux ropes were also reported (Tian et al. 2010).
78 Previous work seems to suggest that such type of RE is more often observed in low-beta solar wind
79 or in the interiors of ICMEs but not particularly prevalent in the leading edge of an ICME since the
80 roughly Alfvénic accelerated flows within field reversal regions, which are regarded as the ‘direct
81 evidence’ of magnetic reconnection, are hard to identify in the front region of the ICME (Gosling
82 2011; Gosling et al. 2005b). However, both numerical simulations and physical models have
83 demonstrated that reconnections could occur in the front BL where MC interacts with the ambient
84 solar wind (Dasso et al. 2006; Wang et al. 2010; Wei, et al. 2003a; Wei, et al. 2003b). Therefore, it is
85 worthwhile to make clear that what the dominant physical process is inside the BL and whether the
86 reconnection process plays an important role.

87

88 The magnetic field is highly related to the local plasma distribution for which the density and
89 temperature are macroscopic manifestations of the plasma velocity distribution function (VDF).
90 Hence, investigation on the VDF is an effective way to diagnose the magnetic field and plasma
91 structure in the solar wind (Gosling et al. 1987; Gosling et al. 2005c; Larson et al. 1997). Generally,
92 the solar wind electron contains the thermal core electron and the suprathermal electron with a
93 breakpoint near ~ 70 eV. Electron at lower energy bands plays an important role in the calculations of
94 electron density and temperature because they can be calculated from the zero- and second-order
95 moments of VDF. The suprathermal electron usually contains two components, a nearly isotropic
96 electron called halo and an electron beam coming directly outward from the Sun called Strahl. The
97 suprathermal electron, especially Strahl electron carrying the heat flux outward from the Sun, has
98 been widely used to diagnose the magnetic field configuration in the solar wind (Gosling et al. 1987;

99 Gosling et al. 2005c; Larson et al. 1997). Electron heat flux dropout in the solar wind is speculated to
100 be an evidence for interplanetary magnetic reconnection (McComas et al. 1989). However, hardly
101 any work has been done to demonstrate whether electron flux variations could be regarded as a
102 sufficient signature for solar wind magnetic reconnection. The enhanced flux of energetic particles,
103 especially the energetic electrons (>100 keV), might also indicate the existence of acceleration
104 processes, such as magnetic reconnection (Lin & Hudson 1971; Oieroset et al. 2002; Wang, et al.
105 2010) or shock (Potter 1981; Tsurutani & Lin 1985). In this paper, we use the Wind data to
106 statistically analyze the proton and electron flux variations in the BL and compare them with those in
107 the MC-driven shock and interplanetary RE and try to reveal the dynamic process inside the BL.

108

109 **2 Data set description and events selection**

110 The WIND 3-D plasma and energetic particle instrument (3DP) provides full three-dimensional
111 distribution of electrons and protons covering a wide range of (time varying) energy bands (Lin et al.
112 1995). The data provided by the electron electrostatic analyzers (EESA), the proton electrostatic
113 analyzers (PESA) and the semiconductor telescopes (SST) will be analyzed. We only analyze the
114 proton flux in the omni direction since the directional proton flux data is not available online. For the
115 electron flux data, we investigate the flux in parallel, perpendicular and antiparallel directions. Since
116 the measurements of electron density and the electron flux at lower energy bands are greatly affected
117 by the instrumental restrictions, we assume that the electron density is equal to the proton density
118 and the electron flux data below 18 eV are not used (see the discussion section). Moreover, in order
119 to facilitate the statistical work, we reconstruct the energy bands at fixed energy to all events; and to
120 avoid the frequently occurred invalid data, we do not use the data provided by the EESA-H and

121 PESA-L experiments. Finally, the electron flux from 18 eV to 500 keV (EESA-L: 18, 27, 42, 65, 103,
122 165, 265, 427, 689 eV; SST-F: 27, 40, 66, 108, 183, 307, 512 keV) and the proton flux from 4 keV to
123 4 MeV (PESA-H: 4, 6, 9, 11, 15, 21, 28 keV; SST-MO: 74, 128, 197, 333, 552, 1018, 2074, 4440
124 keV) will be analyzed.

125 The BL events are identified according to the BL concept and identification criteria (Wei, et al.
126 2003b). The physical characteristics of the tail BL are quite different from the front BL (Wei, et al.
127 2003b; Wei, et al. 2003c; Zuo et al. 2007), and this paper only focus on the flux variations in the
128 front BL detected from 1995 to 2006 (41 events are listed in Table 1a). The interplanetary RE events
129 are chosen from the list provided by Huttunen et al. (2007). Since the time resolution of the EESA
130 and PESA is ~ 98 s, the RE events with too short duration (< 98 s) are excluded (24 events are listed in
131 Table 1c). The MC-driven shock events are selected based on the work of Feng et al. (2011). We use
132 the following criteria to select shock events as ‘MC-driven’ events (23 events are listed in Table 1c):
133 (1) the angle θ between the axe of the MC, adopted by fitting the constant α force-free model to the
134 magnetic fields (Feng et al. 2010), and its leading shock normal is in the range from 65 to 115 degree;
135 (2) the interval between the shock and the beginning of the MC is less than 14 hours.

136 During the statistical work, we quantify the flux variations in the form of $\Delta F = (F_2 - F_1) / F_1$ at each
137 energy band and direction for each event. In the case of the BL events, F_2 is the mean flux inside the
138 BL and F_1 is the mean flux of the nearby upstream solar wind with 30 minutes duration. For RE, F_2
139 is the mean flux inside the RE and F_1 is mean flux of the nearby upstream solar wind with the same
140 duration of the RE. For the shock, F_1 and F_2 are the mean flux of upstream and downstream solar
141 wind respectively with 12 minutes duration and 3 minutes away from the shock discontinuity. The
142 possible influences of our selection criteria and sample method on the final results of flux variations

143 will be discussed in the last section.

144

145 **3 Statistical results**

146 The local magnetic field and plasma parameters of the three types of events (BLs, REs, Shocks)
147 are listed in Table 1. It is found that the magnetic field decreases ($\Delta B_t \sim -16.4\%$) in most of the BL
148 events and plasma is usually compressed ($\Delta N_p \sim 42.9\%$) and heated ($\Delta T_e \sim 5.3\%$, $\Delta T_p \sim 16.6\%$). These
149 phenomena resemble previous work (Wei, et al. 2003b; Wei, et al. 2006) on BL events, and they are
150 quite similar to the RE events despite the somewhat larger temperature increment (ΔB_t , ΔN_p , ΔT_e ,
151 $\Delta T_p \sim -20.1\%$, 35.8% , 10.6% and 27.1% respectively). The average duration of the BLs ($\Delta t \sim 67$
152 minutes) is ~ 18 times longer than that of the REs ($\Delta t \sim 229$ seconds) and the absolute difference of
153 proton velocity in the REs ($\Delta V_p \sim 21.7 \text{ km/s}$) is larger than that in the BLs ($\Delta V_p \sim 12.1 \text{ km/s}$). The
154 MC-driven shocks are usually fast forward shocks across which the magnetic field, proton and
155 electron temperature and plasma speed always increase much (the average changes of ΔB_t , ΔN_p , ΔT_e ,
156 ΔT_p , ΔV_p are $\sim 140.7\%$, 122.2% , 82.9% , 161.3% and 81.5 km/s respectively). It is also noted that
157 there are few strong strength MC-driven shocks. The obtained density compression ratio of the shock
158 is in the range of 1.3-4.6 with a mean value of only 2.2.

159 Figure 2 presents the electron flux variation ΔF averaged over all events in the parallel,
160 anti-parallel, perpendicular direction as well as the omni proton flux variation also averaged over all
161 events. The flux variations (flux decrease or increase) depend both on the direction and the energy.
162 Inside the BL, the core electron flux in the parallel, anti-parallel and perpendicular direction increase
163 consistently and the increment amplitude decreases with energy monotonously from $\sim 30\%$ (at 18 eV)
164 to $\sim 10\%$ (at 70 eV); the increments of suprathermal electron ($100\text{-}700 \text{ eV}$) in the parallel and

165 antiparallel directions are very small ($<4\%$), but it is noted that their standard error are obviously
166 large; the energetic electron ($>100\text{keV}$) also has slight increments in the perpendicular direction; the
167 increments of the proton omni flux fall at higher energy bands but they have a prominence around
168 70keV . In the RE, although the energetic electron in the parallel direction has higher increment with
169 larger standard error, the flux variations have similar behaviors compared with the BL as a whole. By
170 contrast, across the shock, flux behaviors are quite different. The electron flux variations have peak
171 increments ($>200\%$) around $\sim 100\text{eV}$ and decline on both sides; we also note that they have higher
172 increments in the perpendicular direction and the corresponding energy of the peak increment is also
173 higher in the perpendicular direction ($\sim 165\text{eV}$) than in the field-aligned direction ($\sim 65\text{eV}$); the omni
174 proton flux increments decrease monotonously from $\sim 280\%$ (at 4keV) to $\sim 10\%$ (at 4MeV).

175 During the statistical work, it is also found that the correlations of the electron flux variations in
176 parallel and antiparallel directions have a sharp change around 70eV where solar wind magnetic
177 reconnection occurs. Figure 3 provides the correlation coefficients of electron flux variations in the
178 parallel and antiparallel directions. In all events, the core electron has (strong) positive correlations
179 (BL and RE: $r>0.8$; shock: $r>0.6$); while the suprathermal electron in the BL and RE has very low or
180 negative correlations (BL: $r\sim 0$; RE: $r\sim -0.2$), in addition, the correlations are even lower across
181 (downstream to upstream) the RE ($r\sim -0.4$); however, no obvious changes are found across the shock
182 which always has high correlation around 0.8 .

183

184 **4 Explanations for flux variations**

185 Since the compressing and heating effects are quite common inside the BL, RE and across the
186 shock, these effects could account for the presented core electron flux variations. The zero-order

187 moment of the VDF is equal to the mass density. Accordingly, if the VDF has a Maxwellian
188 distribution, the density will behave essentially the same as the flux. Especially, the lower the flux
189 energy is, the more similar behaviors the density and flux have. As is seen in Figure 4, the isotropic
190 increments of electron flux at 15-41eV vary consistently with the density changes in the BL. The
191 final increments of the electron flux at 18eV are also roughly consistent with the average density
192 increments (listed in Table 1a) and previously statistical results (Wei, et al. 2006). Therefore, the
193 enhancements of the core electron flux with high correlation in all three directions could be related to
194 the density increase in the compressed BLs. The core electron flux variation in the REs is similar to
195 the BLs, however, it behaves totally different across the MC-driven shocks. The electron flux
196 increments ascend first and then descend with peak value near ~ 65 eV and ~ 165 eV in the
197 field-aligned and perpendicular directions respectively. Such flux behaviors could not be merely
198 caused by the density increase and increments are also inconsistent with the average density
199 increments. We noted that the increase of electron temperature across the shock is quite higher than
200 that in the BL and RE. Since the ‘moment temperature’ (Burlaga 1995) is calculated from the
201 second-order moment of the VDF, we speculate that the increments of electron flux with hill-like
202 shape are mainly dominated by the heating effect of the shock. This result is consistent with previous
203 observations which show that the inflated electron VDF caused by heating in both the parallel and
204 perpendicular directions is always found downstream of the shock (Fitzenreiter et al. 2003). In
205 addition, according to early researches, for weaker shocks, the electron heating was primarily
206 perpendicular to the magnetic field due to the conservation of magnetic moment (Feldman et al.
207 1983). The present statistical results with higher flux increments in the perpendicular directions
208 could be also supported by such explanations, since many of our selected MC-driven shocks have

209 relatively small density compression ratio.

210

211 As described in the introduction section and the references therein, the bidirectional,
212 unidirectional and absence of Strahl electron could reflect the configurations of closed, open and
213 disconnected magnetic field lines from the Sun respectively (Gosling, et al. 1987; Gosling, et al.
214 2005c; Larson, et al. 1997). Although previous work has speculated their dependences and analyzed
215 their behaviors in the reconnection (Gosling, et al. 2005c; McComas, et al. 1989), there are no
216 sufficient direct relevance established between the electron flux variations and solar wind magnetic
217 reconnection. In our statistical work, we find that the suprathermal electron (100-700eV) flux
218 displays low or even negative correlation between the parallel and antiparallel directions when a
219 spacecraft across the RE. Here we would like to explain why these features are **related to the solar**
220 wind reconnection in some details. As sketched in Figure 5, taking the Strahl electron in ideal case
221 for instance, the intensity of flux is simply normalized by only two arbitrary quantities: 100 (obvious
222 Strahl electron) and 10 (no obvious Strahl electron). The flux status is described by [F0,F180], where
223 F0 and F180 stand for the flux of Strahl electron in the parallel and antiparallel directions
224 respectively. Accordingly, the status of bidirectional Strahl electron, unidirectional Strahl electron in
225 the parallel and antiparallel directions and no obvious Strahl electron could be described by
226 [100,100], [100,10], [10,100] and [10,10] respectively. In cases I, the spacecraft would detect
227 decreased and unchanged Strahl electron in the parallel and antiparallel directions respectively inside
228 the RE, and the increments are [-90,0] ([10,10]-[100,10]). Similarly, the increments in case II, III and
229 IV are [0,90], [0,-90] and [90,0] respectively. Therefore, in statistical analyses, the correlations of the
230 Strahl electron flux variations in parallel and antiparallel directions should be low if the spacecraft

231 encounter the above four cases randomly. Mathematically speaking, both the correlation coefficient
232 and the averaged increments should approach 0. Moreover, across the RE, the increments become
233 $[-90,90]$ in case I, II and $[90,-90]$ case III, IV. We could see that they always reveal anti-correlated
234 relations in the parallel and antiparallel directions. Accordingly, the theoretically computed
235 correlation coefficient is even lower (should be -1) in the statistical work. Certainly, our assumptions
236 are relatively simple, for example, the real flux intensity could not be only two quantities (100 and
237 10), and thus the finally obtained correlation coefficients and mean flux increments might not as
238 ideal as in the analyses. However, the flux variations of suprathermal electron still reveal the
239 properties that the mean increments approach 0 with large stand errors and the correlation
240 coefficients are low (~ 0.2) and lower (~ 0.4) in and across the REs. Other effects, such as particle
241 scattering, could also modify the flux of electron. If so, it should be explained why the correlation of
242 core electron are always higher than the suprathermal electron and why the correlation coefficients
243 change sharply around $\sim 70\text{eV}$. Perhaps the correlation coefficients should change more smoothly if
244 the scattering process plays a dominant role. In addition, since these RE events are not magnetically
245 connected to the Earth's bow shock (Huttunen et al. 2007), the obtained results would not be greatly
246 affected by particle reflection either. Moreover, the correlation coefficients across the MC-driven
247 shock, in which there is no obvious break or reverse of magnetic field line, are always high
248 ($\sim 0.7-0.9$). For these reasons, we tend to regard that the solar wind magnetic reconnection is the best
249 candidate process that could account for the statistically obtained low or negative correlations of
250 suprathermal electron increments in the parallel and anti-parallel directions.

251

252 The energetic electron might come from the Sun directly just as the suprathermal electron, but it

253 should be noted that its flux variations (mean value and stand error) are somewhat different
254 compared with the suprathermal electron. Shocks could also accelerate electron to high energy, but
255 early work (Potter 1981; Tsurutani & Lin 1985) shows that the shock associated accelerations of
256 energetic electron are weak near 1AU. We also find that the energetic electron sometimes shows a
257 pike or step-like increase across the shock with short durations, thus the increments are smoothed by
258 the sample method (3 minutes away and 12 minutes average). These reasons might be responsible for
259 the relatively slight flux increments of energetic electron across MC-driven shock in our statistical
260 work. Previous work (Gosling et al. 2005a) suggests the absence of energetic electron inside the RE.
261 However, observations (Lin & Hudson 1971; Oieroset, et al. 2002) show that energetic electron
262 produced by magnetic reconnection does exist, and the energetic electron could also be found inside
263 the BL (Wang, et al. 2010). As pointed out by Wang, et al. (2010), the MC driving reconnection
264 would prefer to generate complex structures (e.g. diverse magnetic islands) rather than form a single
265 X line in the reconnection region under real solar wind conditions. These seemingly irregular
266 structures could probably play an important role in the generation of energetic electrons (Ambrosiano
267 et al. 1988; Drake et al. 2006; Goldstein, Matthaeus, & Ambrosiano 1986; Matthaeus, Ambrosiano,
268 & Goldstein 1984; Wang, et al. 2010). Actually, for 6 out of 24 RE events and 6 out of 41 BL events,
269 the omni flux increments of ~512 keV electrons exceed 30%. Therefore, the energetic electron might
270 be the shock associated or come from the Sun directly, and it could also be generated by
271 reconnection. However, as analyzed above, the energetic electron accelerated by reconnection seems
272 to be a more reasonable cause for the flux increments inside the REs and BLs.

273

274 **5 Discussion and summary**

275 The data provided by the PESA-L and PESA-H detectors has many gaps and the energy bands
276 are time varying. Due to the lack of reliable and detailed data, it is hard to explain proton flux
277 variations comprehensively or draw a conclusion definitely by only using the omni directional data
278 above 4keV. We still note that the final statistical result of proton in the BL is similar to the previous
279 single-event observation (Wang, et al. 2010) in which a flux peak around 70keV is also found. Since
280 the proton flux increment (~280%) across the MC-driven shock at 4keV is higher than both the
281 density and temperature increments (~122% and 161%, respectively), it is speculated that the proton
282 VDF around 4keV might also be inflated as that of the electron near ~70eV across the shock.

283

284 The electron flux data at low energy bands should be calibrated before use. However, the
285 technical calibrations such as assuming a Gaussian fitted VDF and estimating the spacecraft potential
286 are troublesome. The accuracy is not well guaranteed either. So we do not process the electron flux
287 data below 18 eV. Actually, the electron flux data at these low energy bands seems not to affect the
288 main conclusions of the paper, and neither does the electron flux data provided by EESA-H (1-20
289 keV). Besides, the electron density in the solar wind could also be calibrated by searching a bright
290 'plasma line' in the frequency spectrogram of the wave. It is found that the difference between the
291 proton density and the calibrated electron density in our statistical work is very small, so the proton
292 density is used to replace the electron density.

293

294 As mentioned above, the presented sample method by choosing the mean flux in the specified
295 time range might have some smooth effect on the flux variations. Actually, we also adopted other
296 sample method, such as applying the maximum flux in the same time range to all the events.

297 Although we got more unsmooth results, the main features also resemble the results presented here.
298 We also try to change the criteria of the ‘MC-driving’ shocks, and we find that the main conclusions
299 of the paper are not changed either, despite that the angle between the axe of the MC and shock
300 normal and the interval between the shock and the beginning of the MC would affect the final
301 increments to some extent.

302

303 Magnetic field decrease, density and temperature increase are similar in the RE and BL, and
304 similar flux variation behaviors are found between these two structures. Hence we suggest that the
305 flux variations in the BL are mainly related to the magnetic reconnection process. However, as
306 preliminarily discussed in the introduction section, some researchers pointed out that the roughly
307 Alfvénic accelerated plasma flows--the ‘direct evidence’ (Gosling 2011; Gosling, et al. 2005b), are
308 rarely identified inside the front BL (except two events: 20001003 and 20040724). At first, it should
309 be recognized that no roughly Alfvénic accelerated plasma flows does not mean no magnetic
310 reconnection, since the reconnection jets might not be measured or the generated jets do not meet the
311 referred criteria. Previous simulations (Wang, et al. 2010; Wei, et al. 2006; Wei, et al. 2003a) imply
312 that the BL has strong turbulent property under high magnetic Reynolds number condition ($R_m \sim 10^4$).
313 While, as also suggested by Matthaeus et al. (2003), turbulence should commonly drive reconnection
314 in the solar wind. Inside the BL, the compression of the MC behaves as driving flows that would
315 reduce the characteristic thickness of the local current sheet from $\sim 10^8$ km (in the corona) to $\sim 10^3$ km
316 (in the solar wind). Accordingly, the magnetic Reynolds number could decrease from $\sim 10^{10}$ to $\sim 10^4$.
317 Besides, the magnetic field inside the BL always shows abrupt deflections in the field direction. If
318 the frozen field theorem is locally broken, these conditions are all favored by the potential magnetic

319 reconnection (Wei, et al. 2006). Actually, in many cases, the BL is a complex layer with turbulent
320 and irregular structures, besides, the trajectory of the spacecraft relative to the orientation of RE is
321 not always suitable for the observation. So the roughly Alfvénic accelerated plasma flows that
322 completely meets the reconnection criteria as those reported events might be hard to identify
323 (Gosling, et al. 2005b; Huttunen, et al. 2007; Phan et al. 2006; Tian et al. 2010; Wang, et al. 2010;
324 Xu, Wei, & Feng 2011). In addition, the referred criteria, especially the jets, (Gosling 2011; Gosling,
325 et al. 2005b; Paschmann et al. 1986; Sonnerup & Cahill 1967) are described as ‘a useful guide’
326 (Sonnerup et al. 1981) for the identification of reconnection and have made wonderful achievements
327 in the realm of magnetic reconnection, yet it should still be cautious to use such criteria because they
328 are obtained under the MHD descriptions with the assumption of ideal reconnection model.
329 Remarkably, it is pointed out (Sonnerup, et al. 1981) that such criteria have never been demonstrated
330 to be ‘incontrovertible’. Recent simulations also show that the outflowing reconnection jets could
331 even turn back and link with the inflows to form closed-circulation patterns in turbulent reconnection
332 (Lapenta 2008). Accordingly, reconnection generated plasma flows might not meet the referred
333 criteria strictly in real three-dimensional space. Therefore, it is quite possible that many
334 reconnections inside the BL do occur and the reconnection jets are indeed measured. However, they
335 are excluded by the criteria so that many researchers think there is no reconnection. We do not want
336 to discuss the reconnection criteria further since it is beyond the scope of this paper. Other factors
337 should also be taken into consideration carefully, such as the life span and the evolution of the
338 reconnection itself. As studied previously (Wei, et al. 2003a; Wei, et al. 2003b), the magnetic
339 reconnection might not be ongoing process all the time. After the reconnection occurs, the
340 reconnection conditions would be weakened and the frozen-in condition would be gradually

341 recovered until the local condition is ready for the next potential magnetic reconnection. Since this
342 process might continue to repeat itself, a single spacecraft across the BL might observe the ‘remains’
343 or the ‘preorder’ of magnetic reconnection. For these reasons, the signatures of reconnection, such as
344 the Alfvénic accelerated flows (Gosling, et al. 2005b; Huttunen, et al. 2007; Phan et al. 2006; Tian et
345 al. 2010; Wang, et al. 2010; Xu, Wei, & Feng 2011), might be not prominent to be identified
346 sometimes. However, we have reasons to believe that the electron flux variations would not be
347 affected and could reflect the field topological structure of the magnetic reconnection event to a
348 certain extent.

349

350 In summary, we carry out a statistical study to analyze the proton and electron flux variations
351 inside BL events on reliable energy bands and compare them with those in the RE and across the
352 MC-driven shocks. The results show that the BL is a unique complicated transition layers that
353 displays some reconnection characteristics. The core electron flux behaviors inside the BL and RE
354 are related to the density increase. The hill-like electron flux increments across the shock are mainly
355 dominated by the temperature increase. It is also found that the correlations of the electron flux
356 variations in parallel and antiparallel directions have a sharp change around $\sim 70\text{eV}$ where solar wind
357 magnetic reconnection occurs. The correlation coefficients of the suprathermal electron in the
358 parallel and antiparallel directions are found to be low. Further analyses imply that strong energy
359 dependence and direction selectivity of flux variations could be regarded as an important signature of
360 solar wind reconnection in the statistical point of view.

361

362

363 **Acknowledgement**

364 This work is jointly supported by the National Natural Science Foundation of China (40890162,
365 40904049, 40921063, and 41031066), 973 program 2012CB825601 and the Specialized Research
366 Fund for State Key Laboratories. We thank NASA CDAWEB and Space Sciences Laboratory at UC
367 Berkeley for providing the Wind 3DP and MFI data. Y. Wang thanks T. R. Sun, H. Tian and H.Q.
368 Feng for their helpful discussions.

369

370 **References**

- 371 Ambrosiano, J., Matthaeus, W. H., Goldstein, M. L., & Plante, D. 1988, *J Geophys Res-Space*, 93, 14383
372 Bothmer, V., & Schwenn, R. 1994, *Space Sci Rev*, 70, 215
373 Burlaga, L., et al. 1980, *J Geophys Res-Space*, 85, 2227
374 Burlaga, L., Sittler, E., Mariani, F., & Schwenn, R. 1981, *J Geophys Res-Space*, 86, 6673
375 Burlaga, L. F. 1995, *Interplanetary Magnetohydrodynamics*, Oxford Univ Press, New York
376 Burlaga, L. F., Scudder, J. D., Klein, L. W., & Isenberg, P. A. 1990, *J Geophys Res-Space*, 95, 2229
377 Dasso, S., Mandrini, C. H., Demoulin, P., & Luoni, M. L. 2006, *Astron Astrophys*, 455, 349
378 Drake, J. F., Swisdak, M., Che, H., & Shay, M. A. 2006, *Nature*, 443, 553
379 Fainberg, J., Osherovich, V. A., Stone, R. G., MacDowall, R. J., & Balogh, A. 1996, *Aip Conf Proc*, 382, 554
380 Farrugia, C. J., Fitzenreiter, R. J., Burlaga, L. F., Erkaev, N. V., Osherovich, V. A., Biernat, H. K., & Fazakerley, A. 1994,
381 *Magnetosheath*, 14, 105
382 Farrugia, C. J., et al. 2001, *Adv Space Res*, 28, 759
383 Feldman, W. C., Anderson, R. C., Bame, S. J., Gosling, J. T., Zwickl, R. D., & Smith, E. J. 1983, *J Geophys Res*, 88,
384 9949
385 Feng, H. Q., Wu, D. J., Chao, J. K., Lee, L. C., & Lyu, L. H. 2010, *J Geophys Res-Space*, 115
386 Fitzenreiter, R. J., Ogilvie, K. W., Bale, S. D., & Viñas, A. F. 2003, *J Geophys Res*, 108, 1415
387 Goldstein, M. L., Matthaeus, W. H., & Ambrosiano, J. J. 1986, *Geophys Res Lett*, 13, 205
388 Gosling, J. T. 2011, *Space Sci Rev*, 1, 14
389 Gosling, J. T., Baker, D. N., Bame, S. J., Feldman, W. C., Zwickl, R. D., & Smith, E. J. 1987, *J Geophys Res-Space*, 92,
390 8519
391 Gosling, J. T., Skoug, R. M., Haggerty, D. K., & McComas, D. J. 2005a, *Geophys Res Lett*, 32
392 Gosling, J. T., Skoug, R. M., McComas, D. J., & Smith, C. W. 2005b, *J Geophys Res-Space*, 110, 1107
393 Gosling, J. T., Skoug, R. M., McComas, D. J., & Smith, C. W. 2005c, *Geophys Res Lett*, 32, 5105
394 Huttunen, K. E. J., Bale, S. D., Phan, T. D., Davis, M., & Gosling, J. T. 2007, *J Geophys Res-Space*, 112
395 Janoo, L., et al. 1998, *J Geophys Res-Space*, 103, 17249
396 Lapenta, G. 2008, *Phys Rev Lett*, 100, 235001
397 Larson, D. E., et al. 1997, *Geophys Res Lett*, 24, 1911
398 Lepping, R. P., et al. 2006, *Ann Geophys-Germany*, 24, 215

399 Lepping, R. P., et al. 1997, *J Geophys Res-Space*, 102, 14049
400 Lin, R. P., et al. 1995, *Space Sci Rev*, 71, 125
401 Lin, R. P., & Hudson, H. S. 1971, *Sol Phys*, 17, 412
402 Matthaeus, W. H., Ambrosiano, J. J., & Goldstein, M. L. 1984, *Phys Rev Lett*, 53, 1449
403 Matthaeus, W. H., Dmitruk, P., Oughton, S., & Mullan, D. 2003, *Solar Wind Ten, Proceedings*, 679, 427
404 McComas, D. J., Gosling, J. T., Hammond, C. M., Moldwin, M. B., Phillips, J. L., & Forsyth, R. J. 1994, *Geophys Res*
405 *Lett*, 21, 1751
406 McComas, D. J., Gosling, J. T., Phillips, J. L., Bame, S. J., Luhmann, J. G., & Smith, E. J. 1989, *J Geophys Res*, 94, 6907
407 Oieroset, M., Lin, R. P., Phan, T. D., Larson, D. E., & Bale, S. D. 2002, *Phys Rev Lett*, 89
408 Osherovich, V. A., Farrugia, C. J., Burlaga, L. F., Lepping, R. P., Fainberg, J., & Stone, R. G. 1993, *J Geophys Res-Space*,
409 98, 15331
410 Paschmann, G., Papamastorakis, I., Baumjohann, W., Sckopke, N., Carlson, C. W., Sonnerup, B. U. O., & Luhr, H. 1986,
411 *J Geophys Res-Space*, 91, 1099
412 Phan, T. D., et al. 2006, *Nature*, 439, 175
413 Potter, D. W. 1981, *J Geophys Res*, 86, 11111
414 Sonnerup, B. U., & Cahill, L. J. 1967, *J Geophys Res*, 72, 171
415 Sonnerup, B. U. O., et al. 1981, *J Geophys Res-Space*, 86, 49
416 Tian, H., Yao, S., Zong, Q. G., He, J. S., & Qi, Y. 2010, *Astrophys J*, 720, 454
417 Tsurutani, B. T., & Lin, R. P. 1985, *J Geophys Res*, 90, 1
418 Wang, Y., Wei, F. S., Feng, X. S., Zhang, S. H., Zuo, P. B., & Sun, T. R. 2010, *Phys Rev Lett*, 105, 195007
419 Wei, F. S., Feng, X. S., Yang, F., & Zhong, D. K. 2006, *J Geophys Res-Space*, 111, 3102
420 Wei, F. S., Hu, Q., Feng, X. S., & Fan, Q. L. 2003a, *Space Sci Rev*, 107, 107
421 Wei, F. S., Liu, R., Fan, Q. L., & Feng, X. S. 2003b, *J Geophys Res-Space*, 108, 1263
422 Wei, F. S., Liu, R., Feng, X. S., Zhong, D. K., & Yang, F. 2003c, *Geophys Res Lett*, 30, 2283
423 Xu, X., Wei, F., & Feng, X. 2011, *J Geophys Res-Space*, 116, 5105
424 Zuo, P. B., Wei, F. S., Feng, X. S., & Yang, F. 2007, *Sol Phys*, 242, 167
425
426

Figure captions

427 Figure 1 Wind measurements of the magnetic field strength, latitude angle, azimuth angle, proton
428 density, temperature, velocity, pressure and plasma beta value on 1997 May 15. The shock is
429 indicated by the dotted lines; the dashed lines marked by M_f and G_f represent the BL region; the
430 following MC body is also indicated.

431

432 Figure 2 Normalized mean flux variations with error bars at each energy band. First row: BL; second
433 row: RE; third row: MC-driven shock; first column: electron flux in the parallel direction; second
434 column: electron flux in the perpendicular direction; third column: electron flux in the antiparallel
435 direction; fourth column: proton flux in the omni direction.

436

437 Figure 3 Correlation coefficients of electron increments in the parallel and anti-parallel directions. In
438 the BL: red, in the RE: green, across the MC-driven shock: blue, across the RE: black.

439

440 Figure 4 Plasma and magnetic field conditions near a BL on 05/27/1996 (marked by M_f and G_f ,
441 dashed lines). From top to bottom: the magnitude of magnetic field, electron density, electron flux in
442 parallel, perpendicular and antiparallel directions. The color lines represent different energy bands at
443 15 eV (black), 21 eV (blue), 29 eV (yellow) and 41 eV (red) respectively.

444

445 Figure 5 Schematic plot of magnetic field disconnection (possible reconnection) of 4 cases and the
446 possibly following MC.

Table 1a. Typical magnetic cloud boundary layers observed by WIND

No. ^a	DATE ^b	Start ^c	Dur ^d	ΔB_t^e	$ \Delta V_p ^f$	ΔN_p^g	ΔT_e^h	ΔT_p^i
1	19950208	0252	31	-8.09	6.58	17.31	-4.57	-4.28
2	19950403	0629	75	-12.91	1.70	40.91	0.22	19.85
3	19950822	2036	61	-3.76	1.53	10.24	-2.40	5.61
4	19951018	1820	41	-22.24	2.38	4.15	-0.62	1.94
5	19960527	1210	152	-21.89	2.09	93.15	-3.45	7.16
6	19960701	1546	100	-17.55	9.92	4.22	-1.03	-0.47
7	19970411	0524	30	8.21	0.36	-8.47	-2.69	21.94
8	19970421	1152	13	-30.56	2.36	7.40	-2.37	12.08
9	19970515	0732	139	-16.73	32.64	-22.53	18.07	154.98
10	19970715	0844	21	-36.69	3.50	88.51	0.16	11.94
11	19970803	1005	226	-4.81	12.72	133.46	-16.20	-1.53
12	19970918	0255	57	-18.28	7.70	40.77	2.92	17.14
13	19971107	1438	59	-1.20	0.45	21.52	-7.61	-0.97
14	19971122	1448	22	-15.12	23.70	49.51	9.73	53.52
15	19980502	1233	21	-4.18	5.43	30.12	1.24	3.71
16	19980624	1611	31	-18.36	7.02	40.40	-3.93	-9.90
17	19980820	0450	263	-34.37	35.43	104.60	-6.23	21.38
18	19981108	2250	79	-11.65	5.32	39.97	17.13	23.54
19	19990218	1149	33	-23.58	23.58	41.22	26.70	-2.38
20	19990809	0756	142	-7.00	3.47	30.88	18.78	-6.21
21	20000220	0155	193	-39.13	4.08	55.08	17.96	-27.99
22	20001003	1634	44	-8.62	19.14	5.86	17.81	55.14
23	20010421	2347	25	-13.83	1.40	30.07	10.91	11.76
24	20010710	1638	92	-5.55	4.90	-0.30	2.92	15.44
25	20020319	2127	131	-18.96	5.86	2.80	4.54	42.80
26	20020324	0305	14	-21.83	4.72	123.21	23.79	32.09
27	20020418	0419	20	-19.89	17.98	17.93	4.49	61.71
28	20020519	0246	34	-33.36	14.79	43.60	12.33	5.87
29	20020801	1119	26	-22.67	9.31	48.73	25.64	23.08
30	20020802	0604	71	-6.07	1.46	21.70	1.64	18.36
31	20020903	0250	71	4.21	9.44	33.34	18.89	-7.48
32	20040404	0205	18	-18.46	33.65	191.12	1.19	62.40
33	20040722	1258	56	-28.26	27.65	36.16	15.41	-14.50
34	20040724	1129	27	-9.27	12.78	-10.59	-5.54	10.99
35	20040829	1830	28	-18.18	33.78	0.17	-1.02	0.54
36	20041109	1937	53	-41.59	5.98	68.43	20.51	13.83
37	20050520	0604	42	-17.01	2.46	29.97	-7.81	14.32
38	20050612	1441	21	-44.36	81.13	54.60	-2.16	10.77
39	20051231	1233	76	-37.93	6.83	187.31	16.98	7.20
40	20060205	1759	63	3.36	0.57	5.47	-10.34	-13.15
41	20060413	2023	41	-3.65	8.08	46.47	5.87	29.96
AVERAGE			67	-16.39	12.05	42.89	5.31	16.64

Table 1b. Selected solar wind reconnection exhausts observed by WIND

No. ^a	DATE ^b	Start ^c	Dur ^d	ΔB_t^e	$ \Delta V_p ^f$	ΔN_p^g	ΔT_e^h	ΔT_p^i
1	19971116	164250	220	-38.96	11.13	157.35	30.76	96.31
2	19980416	005434	198	2.27	17.01	-26.45	2.55	96.76
3	19980821	202036	240	-22.31	9.24	37.94	16.54	82.14
4	19980917	033315	109	-14.52	16.27	28.77	-0.15	29.06
5	19990218	102624	218	-23.31	56.20	213.91	63.95	7.90
6	19990615	143235	108	-13.32	16.82	42.82	13.23	91.98
7	19990626	054600	550	-25.24	7.95	29.85	20.53	2.85
8	19990728	043559	189	-24.44	6.29	39.33	1.72	49.62
9	19990810	183820	356	-43.70	2.26	29.98	15.48	16.78
10	19990919	091004	266	-30.09	20.71	24.34	1.90	5.43
11	20000419	035916	194	-39.35	18.40	15.77	10.10	13.30
12	20010617	163023	157	-19.27	38.24	48.55	16.36	1.74
13	20020202	035725	260	-32.48	49.74	65.86	28.72	54.89
14	20020419	004130	300	-9.55	36.29	-14.35	-3.54	10.59
15	20020628	152632	333	-9.36	14.23	22.16	5.92	-11.21
16	20030302	210955	107	-32.84	11.52	6.96	4.90	27.66
17	20040724	115110	235	7.41	62.34	5.42	0.87	45.34
18	20040826	092250	175	-12.69	11.46	-1.11	-3.96	32.22
19	20040914	212651	121	-20.80	60.91	36.30	12.67	-15.88
20	20040919	064100	670	-4.55	12.89	76.63	9.34	5.24
21	20041008	070545	130	-3.13	13.19	13.88	-1.56	6.86
22	20041011	152342	134	-18.82	16.04	-3.39	4.06	-2.68
23	20041029	024531	119	-38.80	9.63	0.77	0.98	1.80
24	20041206	022056	115	-14.50	0.16	2.70	1.95	2.33
AVERAGE			229	-20.09	21.65	35.58	10.56	27.13

Table 1c. Selected leading shocks ahead of magnetic cloud observed by WIND

No. ^a	DATE ^b	Start ^c	ΔB_t^e	$ \Delta V_p ^f$	ΔN_p^g	ΔT_e^h	ΔT_p^i
1	19950822	1256	85.45	42.38	197.09	14.06	99.64
2	19970109	0052	208.79	28.07	118.19	2.41	139.35
3	19970515	0115	150.20	74.66	89.82	53.27	103.76
4	19970715	0215	19.50	9.90	63.46	10.77	22.35
5	19971010	1557	64.41	24.90	62.48	4.70	27.70
6	19971122	0912	198.94	98.79	144.61	75.63	168.50
7	19980304	1102	84.05	41.99	70.94	41.41	40.19
8	19981018	1929	128.17	30.16	89.00	19.93	57.42
9	20000811	1849	106.38	113.98	90.60	56.96	154.63
10	20010319	1133	107.18	47.99	67.30	70.81	60.64
11	20010404	1441	59.08	211.11	146.90	123.27	327.35
12	20010421	1529	80.23	27.70	115.75	60.64	60.14
13	20011031	1347	64.20	68.53	210.07	54.84	301.31
14	20011124	0454	86.78	75.84	33.69	29.39	46.66
15	20020518	1946	158.76	160.83	202.78	240.26	259.96
16	20020801	0519	57.15	100.17	129.64	34.11	296.22
17	20040724	0531	140.13	68.46	168.05	192.04	267.61
18	20041107	1759	123.46	160.31	142.38	90.91	89.20
19	20050515	0210	484.94	298.62	358.26	469.96	803.67
20	20050612	0648	379.41	37.37	30.07	59.08	48.23
21	20050614	1756	253.53	82.10	78.87	107.21	213.60
22	20060413	1121	113.57	35.12	57.57	45.34	79.13
23	20071119	1722	82.14	34.85	142.13	49.76	42.87
AVERAGE			140.72	81.47	122.16	82.90	161.31

457

458

459 NOTE:

460 a Event number

461 b The date of event, formatted as YearMonthDay.

462 c The beginning time of the event, formatted as HourMinute in Table 1a and Table 1c;
463 HourMinuteSecond in Table 1b (UT)

464 d Event duration (Table 1a: minute; Table 1b: second)

465 e The change of total magnetic field (%)

466 f The absolute difference of proton velocity (km/s)

467 g The change proton of density (%)

468 h The change of electron temperature (%)

469 i The change of proton temperature (%)

470 The obtained changes of local plasma and magnetic parameters are similar to the flux variations

471 described in the second section of the paper. They have the same time ranges as the flux variations to

472 each event. (Changes of BL: BL to upstream solar wind; changes of RE: RE to upstream solar wind;

473 changes of shock: downstream to upstream solar wind)

Figures

Figure 1

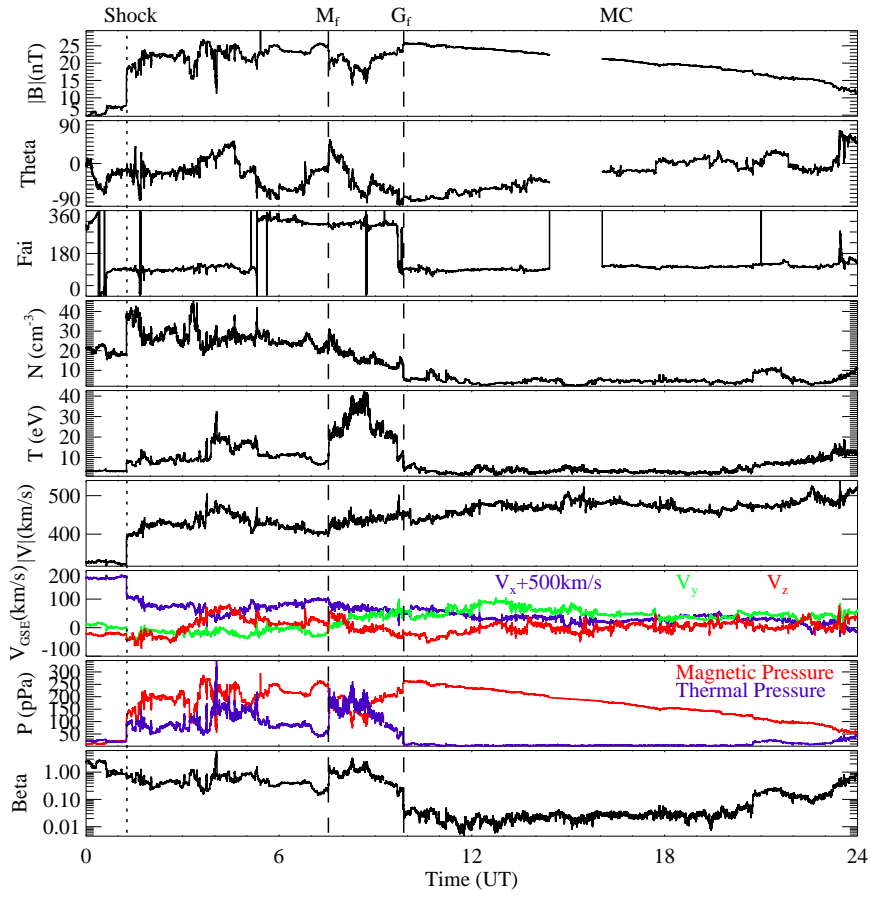


Figure 2

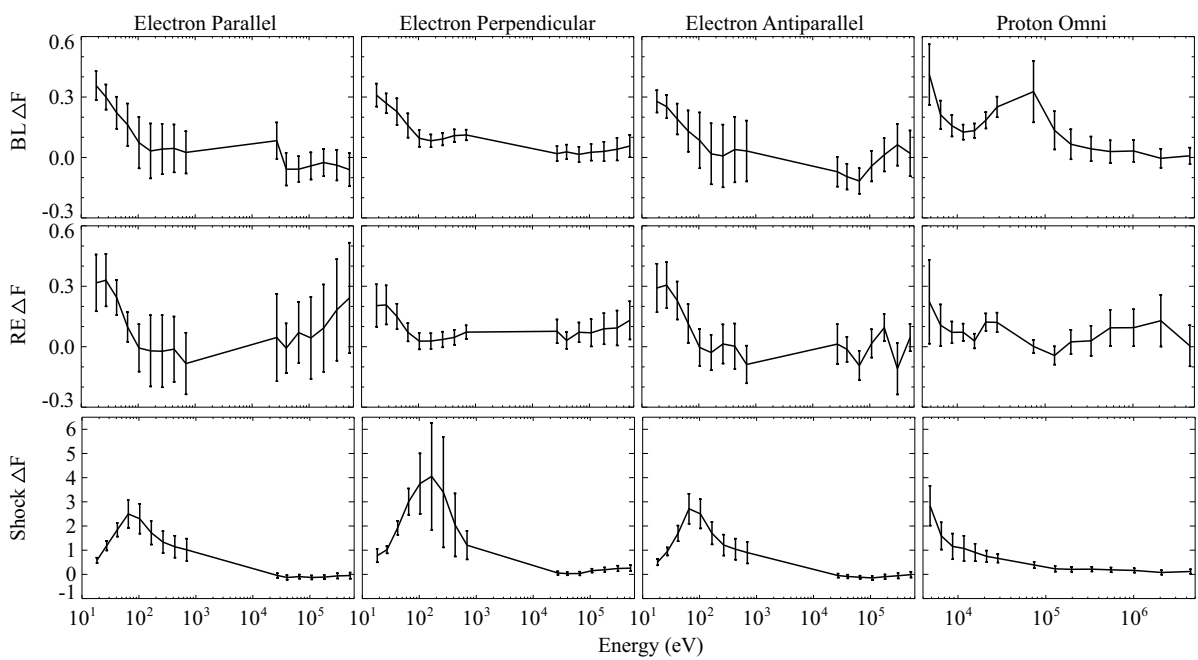


Figure 3

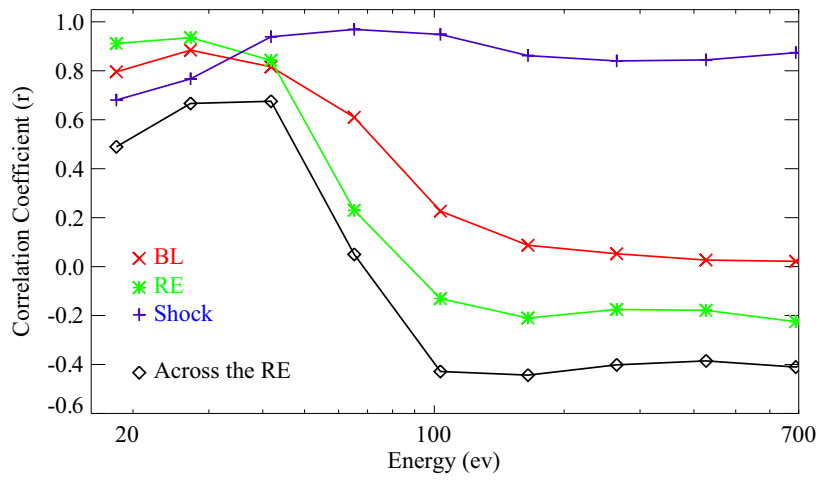


Figure 4

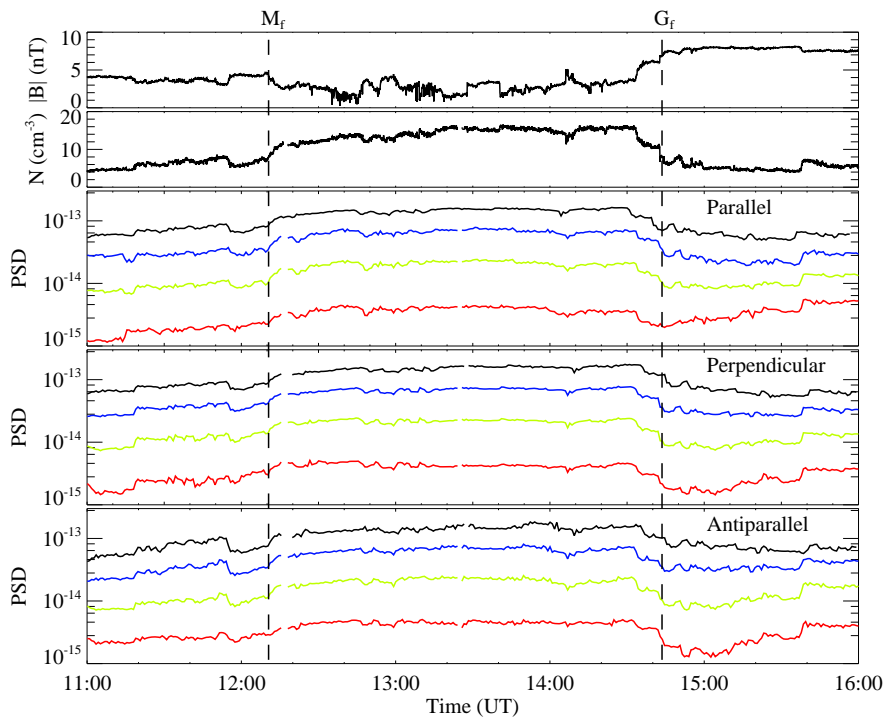


Figure 5

